Journal of Materials Chemistry B

Accepted Manuscript

ROYAL SOCIETY OF CHEMISTRY

www.rsc.org/materialsB

Novel methotrexate prodrug-targeted drug delivery system based on PEG-lipid-PLA hybrid nanoparticles for enhanced anticancer efficacy and reduced toxicity of mytomycin C

Yang Li, [ac] Hongjie Wu, [b] Mengmeng Jia, [a] Conghui Yuan, [a] Ying Chang, [a] Zhenqing Hou, [a,*] Lizong Dai [a,*]

[a] College of Materials, Xiamen University, Xiamen 361005, China

[b] Department of Pharmacy, School of Pharmaceutical Sciences, Xiamen University, Xiamen 361002, China

[c] Department of Chemistry, College of Chemistry & Chemical Engineering, Xiamen University, Xiamen 361005, China

* Corresponding authors.

E-mail addresses: lzdai@xmu.edu.cn (L. Dai), houzhenqing@xmu.edu.cn (Z. Hou),

Tel. +86-592-2186178. Fax: +86-592-2183508

ABSTRACT: In this present study, we established the novel MTX prodrug-targeted and MMC-loaded PLA-lipid-PEG hybrid NPs (PEG-PE-PLA NPs) using a double emulsion-solvent evaporation method by the introduction of both anticancer drugs moiety of the MMC-soybean phosphatidyhlcholine complex (MMC-SPC) and DSPE-PEG-MTX, in which MTX prodrug can be exploited as a targeting ligand. The prepared MTX-PEG-PE-PLA NPs/MMC-SPC presented a spherical shape, a small particle size (219.6 ± 2.1 nm) with a narrow particle size distribution**,** a high MMC encapsulation efficiency (90.5 ± 3.0 %) and a sustained/pH-controlled MMC release. The advantage of the new drug delivery systems is that the two anticancer drugs moiety can coordinate the early-phase targeting effect with the late-phase anticancer effect. In vivo pharmacokinetics after intravenous administration of the MTX-PEG-PE-PLA NPs/MMC-SPC indicated a prolonged systemic circulation time of MMC. More importantly, the MTX-PEG-PE-PLA NPs/MMC-SPC exhibited a significant accumulation of MMC in the nuclei as the site of MMC action, which was indicative of the enhancement of anticancer activity. Such a design of drug delivery systems may open up a new horizon for targeted delivery and sustained/controlled release of MMC.

Introduction

Mitomycin C (MMC), as a powerful anticancer and antibiotic agent by inhibiting DNA synthesis and nuclear division, [1,2] has been extensively used to treat various cancer. [3] MMC is a poor substrate for P-glycoprotein and retains activity against many types of P-glycoprotein-mediated multidrug resistant tumor cells. [4-7] However, the vital obstacle encountered with the efficacy of MMC was the narrow therapeutic index with severe side effects such as kidney toxicity, on the other hand, once intravenously administrated, hydrophilic MMC can be easily subject to fast degradation in therapeutic drug delivery. [8,9]

Nanoscaled drug delivery systems (NDDS) provide an innovative platform for anticancer drugs delivery due to their remarkable pharmacokinetics and biodistribution properities. [10] Thus far, several NDDS including liposomes, polymeric NPs, inorganic NPs, micelles, dendrimers and carbon nanotubes have successfully entered preclinical development in animals or even clinical trials in patients. [11] Recently, a series of work have been developed using liposomes [7,12] or phytosomes [13] for MMC delivery. However, these NDDS, may not be applicable for targeted MMC delivery due to easy drug leakage or poor drug selectivity during circulation.

In our previous work, we increased the lipophilicity and stability of MMC in vitro and in vivo by taking the advantage of phospholipid to prepare the MMC-soybean phosphatidyhlcholine complex (MMC-SPC) via the hydrogen bonds, van der Waals forces or electrostatic interactions. [13,14] Thus far, the supramolecular chemistry was widely used in the design of novel drug preparation or new drug delivery systems.

[15,16] On the one hand, the drug-phopholipid complex via supramolecular chemistry was a key to bridge the conventional and novel drug preparation to improve the safety and efficacy of anticancer drugs. [15,17,18] On the other hand, the self-assembled polymer-lipid hybrid NDDS via supramolecular chemistry have been designed to merge the best of both polymer-based and lipid-based worlds and attracted an increasing interest for drug and gene delivery. [19,20] The encouraging results inspired our motivation of selecting the drug-phopholipid complex as a drug preparation and adopting the polymer-lipid hybrid NPs as a drug delivery system for anticancer drug delivery to achieve efficient encapsulation, prolonged circulation and sustained release.

To improve the encapsulation and preserve the stability of MMC, we used the MMC-SPC complex to act as a drug preparation. Moreover, the drug preparation could reduce drug loss and block drug release to some extent before reaching the target site. To protect the MMC-SPC complex from the physical interactions with the plasma proteins and red blood cells, the polymer-lipid hybrid NPs were served as a protective barrier designed with a core-layer-shell structure: (1) an inner reservoir core, which was hydrophobic PLA to encapsulate the MMC-SPC complex, (2) an interface lipid layer, which was amphiphilic PE to stabilize the NPs structure, promote the cell uptake, and more importantly, control the drug release. [21] (3) an outer protective shell, which was hydrophilic PEG to evade the reticuloendothelial system (RES) while extending the circulation time. Triggered drug release previously reported in our novel NDDS would be likely to become a central strategy for targeted

drug delivery. [22] Despite some advantages of the MMC-phopholipid complex-loaded pH-sensitive polymer-lipid hybrid NPs, the urgent mission still remained regarding how to guide these NPs to the site of interest and improve their therapeutic efficiency.

Folic acid (FA) is an attractive targeting ligand, as the FA receptor has been found to be overexpressed on the surface of a wide variety of cancer cells, including ovarian, lung, breast, kidney, brain, endometrial, and colon cancer cells. [23] Owing to the structural similarity, Methotrexate (MTX) can enter cells through similar transport systems as FA. [24,25] Thus, we hypothesized that using an extensively used anticancer drug MTX as a targeting ligand in advance to allow the polymer-lipid hybrid NPs to achieve two goals: preferential accumulation at the tumor site and enhanced internalization in the tumor cells by a dual mode [26] (active plus passive) targeting strategy. In this paper, we synthesized the DSPE-PEG-MTX for the surface functionalization of the PEG-PE-PLA NPs (Fig. 1A), and proposed a novel platform of MTX prodrug targeted and MMC loaded PEG-PE-PLA NPs (Fig. 2A). The synergistic effect of MMC as a therapeutic anticancer agent with the assistance of MTX as a targeting ligand significantly contributed to cell death, enhancing the therapeutic efficacy (Fig. 2B).

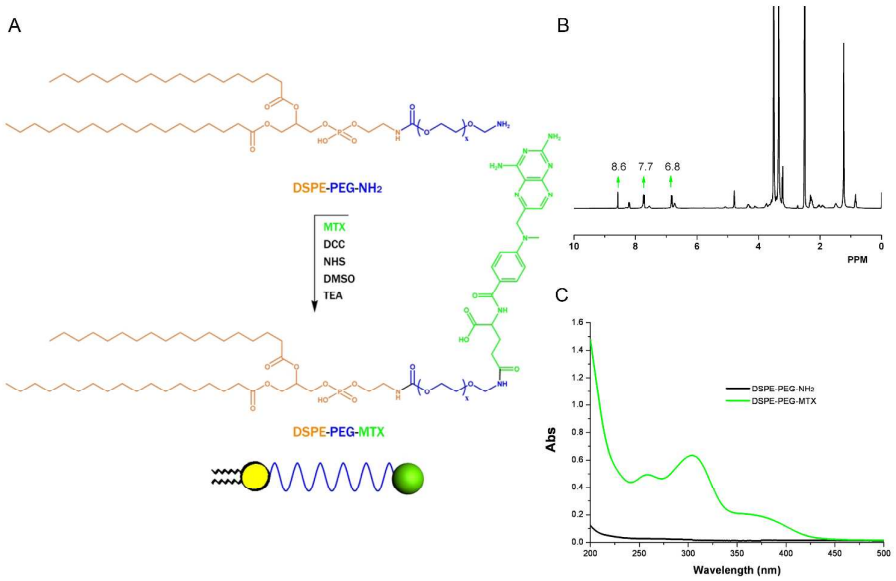

Fig. 1 (A) Synthetic scheme of DSPE-PEG-MTX. (B) NMR analysis of DSPE-PEG-MTX. (C) UV-Vis analysis of DSPE-PEG-MTX.

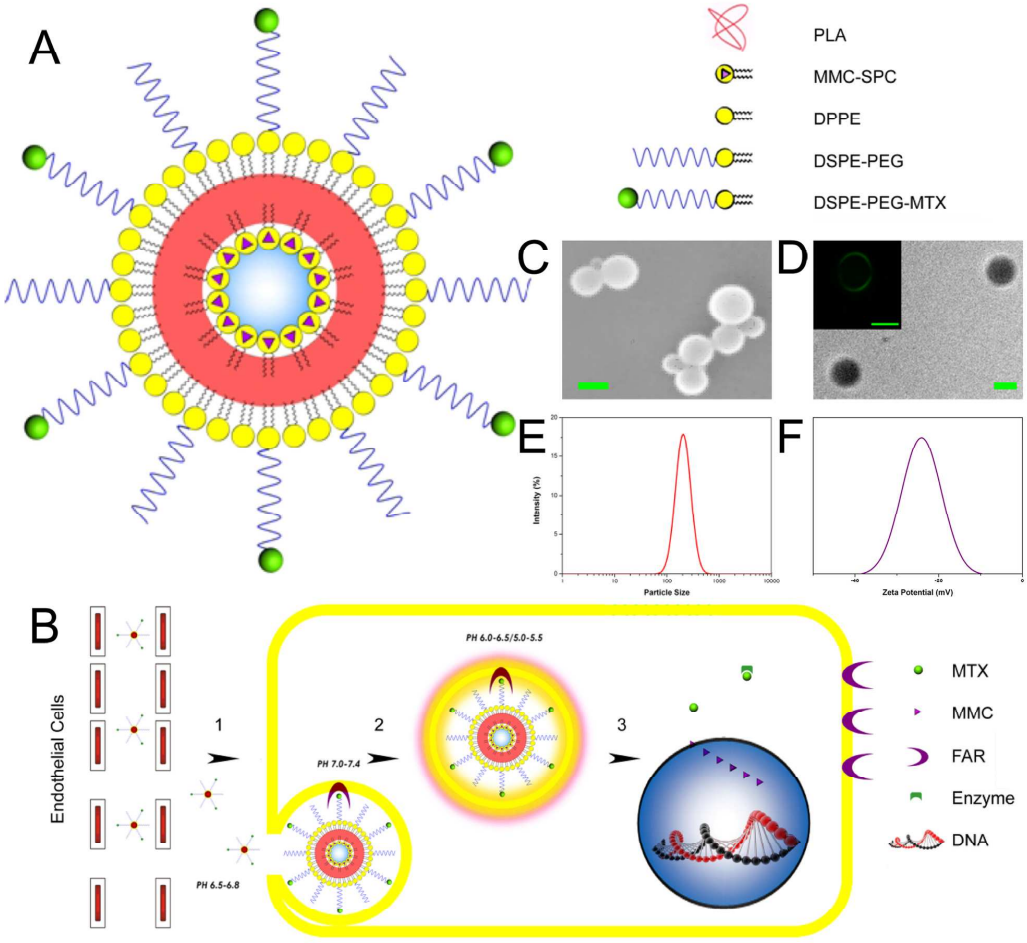

Fig. 2 Illustrations of the preparation of the MTX-PEG-PE-PLA NPs/MMC-SPC and their targeted drug delivery. (A) Illustration of the MTX-PEG-PE-PLA NPs/MMC-SPC. (B) Once intravenously administrated, the long-circulating NPs: (1) were accumulated at the tumor site via the enhanced permeability and retention (EPR) effect, (2) were internalized by the tumor cells via FA receptor-mediated endocytosis, (3) released a first drug (MMC) which was delivered to the nuclei. Inside the cell, a second drug (MTX) might also be released. (C) SEM image. Scale bars = 150 nm. (D) TEM image. Scale bars = 150 nm. Inset: LCSM image of the FITC-MTX-PEG-PE-PLA NPs/MMC-SPC. Scale bars = 2.5 μm. (E) Particle size distribution. (F) Zeta potential distribution.

To our best knowledge, this was also the first report that the anticancer drug-phopholipid complex was introduced into the polymer-lipid hybrid NPs to increase the encapsulation efficiency and reduce the drug release. Thus far, the systematic evaluation of MTX prodrug acting as a targeting ligand in vitro and in vivo has not been reported before. Our MTX prodrug targeted and MMC loaded PEG-PE-PLA NPs platform was expected to improve therapeutic efficacy and reduce the side effects of MMC.

Materials and methods

Materials

Mitomycin C (MMC, purity grade = 99.5%) was purchased from Hisun Pharmaceutical Co., Ltd. (Zhengjiang, China). Soybean phosphatidylcholine (SPC) was provided by Lipoid GmbH (Ludwigshafen, Germany). Poly(D,L-lactide) (PLA, 10 kDa) were provided by Daigang BIO Engineer Co., Ltd. (Shandong, China). 1,

2-dipalmitoyl-sn-glycero-3-phosphoethanolamine (DPPE) was purchased from Corden Pharma Switzerland LLC (Liestal, Switzerland). 1, 2-distearoyl-sn-glycero-3-phosphoethanolamine-N-amino(polyethylene glycol)-2000 (DSPE-PEG-NH_2) and 1, 2-distearoyl-sn-glycero-3-phosphoethanolamine-N-carboxy (polyethylene glycol)-2000 (DSPE-PEG-COOH) were purchased from Avanti Polar Lipids (Alabaster, AL, USA). Methotrexate (MTX) and folate (FA) were purchased from Bio Basic Inc. (Markham, Ontario, Canada). N,N'-dicyclohexylcarbodiimide (DCC) and N-Hydroxysuccinimide (NHS) were purchased from Sigma-Aldrich (St. Louis, MO, USA). Dimethyl sulfoxide (DMSO), dichloromethane (DCM), tetrahydrofuran (THF) and triethylamine (TEA) were obtained from Sinopharm Chemical Reagent Co., Ltd. (Shanghai, China). DiD, DiR and Lysotracker green were from Molecular Probes Inc. (Eugene, OR, USA). Rhodamine phalloidin was from Invitrogen (Carlsbad, CA). Cell Counting Kit-8 (CCK-8) was purchased from Dojindo. Molecular Technologies, Inc. (Rockville, MD, USA). Dialysis bag (Mw = 8, 000 to 12, 000 Da) was ordered from Greenbird Inc. (Shanghai, China). Fetal bovine serum (FBS) was purchased from Gibco Life Technologies (AG, Switzerland). 0.25% Trypsin-EDTA and Penicillin-streptomycin solution was from Invitrogen. Other chemicals were all of analytic grade and were used without further purification. All solvents used in this study were HPLC grade. HeLa cells, A549 cells, Caco-2 cells and MC 3T3-E1 cells were provided by American Type Culture Collection (ATCC).

Synthesis of DSPE-PEG-MTX

Firstly, in a flask, 5 mg of MTX, 5 mg of DCC and 2.5 mg of NHS were co-dissolved

in DMSO and stirred for 1 h under a nitrogen atmosphere to prepare the NHS-activated MTX. Then 10 mg of DSPE-PEG-NH_2 was dissolved in DMSO and TEA and added to the flask. Lastly, the reaction mixture was stirred for an additional 48 h under a nitrogen atmosphere and filtered for remove of white precipitation. The prepared DSPE-PEG-MTX was added into PBS and dialyzed against PBS/DI water for 120 h to completely remove excess of MTX and other byproducts, then the suspensions were lyophilized at -80 °C for 24 h.

Preparation of MTX-PEG-PE-PLA NPs/MMC-SPC

MMC-SPC complex was prepared by a solvent evaporation method as previously reported in our work. [13] MTX-PEG-PE-PLA NPs/MMC-SPC were formulated via a modified double emulsion solvent-evaporation technique. [19,27] In brief, weighed amount of MMC-SPC (mol ratio of MMC: SPC = 1:1) was reconstituted in DI water to form the internal water phase. PLA were dissolved in DCM to form the oil phase. DPPE, DSPE-PEG-COOH (DSPE-PEG) and DSPE-PEG-MTX (weight ratio of DPPE: DSPE-PEG: DSPE-PEG-MTX = 2:1:0.6) were dispersed in DI water by sonication to form the external water phase. The internal water phase was added into the oil phase. The mixture was emulsified by sonication in an ice-water bath; a first W/O emulsion was formed. Next, the emulsified mixture was added into the external water phase, subsequently the mixture was vortexed and then sonicated; a double emulsion was formed. The organic solvent was evaporated from the emulsion by magnetic stirring and further removed by evaporation under reduced pressure in a rotary evaporator. The suspension was centrifuged at 15, 000 rpm for 20 min at 4 °C

to collect the MTX-PEG-PE-PLA NPs/MMC-SPC. After washing with DI water three times, the MTX-PEG-PE-PLA NPs/MMC-SPC were resuspended in DI water with 3% w/w sucrose as cryoprotectant and lyophilized at -80 ℃ for 24 h. The lyophilized products were stored at 4 ℃ for future use. Additionally, on the one hand, the PEG-PE-PLA NPs/MMC-SPC were prepared using the identical procedure with DSPE-PEG-MTX replaced by DSPE-PEG at the equivalent DSPE molar for comparison of most of the experiments. On the other hand, the MTX-PEG-PE-PLA NPs/MMC or MTX-PEG-PE-PLA NPs/MMC+SPC were respectively prepared using the same way except that MMC-SPC was replaced by MMC or the physical mixture of MMC and SPC at the equivalent MMC or SPC mass for comparison of in vitro drug release. Furthermore, the PEG-PE-PLA NPs/SPC as well as MTX-PEG-PE-PLA NPs/SPC was also respectively prepared using the same way with MMC-SPC replaced by SPC at the equivalent SPC mass for comparison of cytocompatibility and hemocompatibility.

NMR, UV-Vis and XRD analysis

DSPE-PEG-MTX was dissolved in the deuterated DMSO and ^{1}H NMR spectrum was recorded with a Bruker AV400 MHz NMR spectrometer (Billerica, MA, USA). Alternatively, DSPE-PEG-MTX was analyzed by UV-Vis (DU800 Beckman Coulter, Brea, California) from 200 to 500 nm. DSPE-PEG-NH_2 was used for comparison.

The physical state of MMC drug in the PEG-PE-PLA NPs/MMC-SPC was investigated by XRD (Phillips X'pert Pro Super, Panalytical, Almelo, The

Netherlands). MMC was used for comparison. The results were included in Fig. S2C†.

Drug encapsulation efficiency

3 mg of lyophilized MTX-PEG-PE-PLA NPs/MMC-SPC was dissolved in 1 mL of DCM. After evaporating DCM, 3 mL of the mobile phase (HPLC grade methanol/water (35/65, v/v)) was added to dissolve MMC and filtrated by 0.45 μm filter membrane. The determination of MMC was performed by a HPLC method. A Symmetry C18 column (250 mm × 4.6 mm, 5 μ m, Waters Associates, Milford, MA, USA) was used. UV-Vis detection was performed at 365 nm. The encapsulation efficiency was calculated by the percentage of the actual amount of MMC encapsulated into the NPs to the initial total amount of MMC used in the fabrication of the NPs. The PEG-PE-PLA NPs/MMC-SPC, MTX-PEG-PE-PLA NPs/MMC or MTX-PEG-PE-PLA NPs/MMC+SPC were used for comparison.

Particle size, polydispersity index (PDI), zeta potential and morphology

The average particle size and PDI of the MTX-PEG-PE-PLA NPs/MMC-SPC were determined by DLS using a Malvern Zetasizer Nano-ZS (Malvern Instruments, Worcestershire, UK). The zeta potential of the MTX-PEG-PE-PLA NPs/MMC-SPC was evaluated by ELS with Zetaplus (Brookhaven Instruments Corporation, Holtsville, NY, USA). Particle size was evaluated by intensity distribution. The morphology of the MTX-PEG-PE-PLA NPs/MMC-SPC was visualized by SEM

(LEO 1530VP, Oberkochen, Germany) operating at 20 kV and TEM (JEM 1400, JEOL, Tokyo, Japan) operating at 200 kV.

In vitro stability tests

A short-term stability test. The lyophilized MTX-PEG-PE-PLA NPs/MMC-SPC were suspended in PBS (pH 7.4) or 10% plasma/heparin in PBS and incubated at 37 °C for 120 h. The particle size was assayed at 24 h intervals by DLS.

A long-term stability test. The storage stability of the lyophilized MTX-PEG-PE-PLA NPs/MMC-SPC was performed at 4 or 25 °C for 3 months. At the predesigned time intervals, the particle size, zeta potential and encapsulation efficiency were assayed.

In vitro drug release

The release of MMC from the MTX-PEG-PE-PLA NPs/MMC-SPC was determined by a dialysis technique using a dialysis bag (Mw = 8, 000-12, 000 Da). The lyophilized MTX-PEG-PE-PLA NPs/MMC-SPC were dialyzed against PBS (1/15 M, pH 7.4, 6.5, 5.5) at 37 °C. At the predesigned time, 2 mL of the release medium was completely withdrawn and subsequently replaced with the 2 mL of fresh PBS. The release of MMC was determined by a HPLC method as described above. In addition, the release of the free MMC, PEG-PE-PLA NPs/MMC-SPC, MTX-PEG-PE-PLA NPs/MMC or MTX-PEG-PE-PLA NPs/MMC+SPC was investigated for comparison.

Hemolysis Assay

0.8 mL of the freshly collected whole blood was then centrifuged to isolate the red blood cells (RBCs). The RBCs were washed five times with sterile isotonic PBS. The washed RBCs were suspended in 7.5 mL of PBS in an ice bath and 0.5 mL was added to 0.5 mL of MMC drug-free NPs suspended in PBS at a concentration of 75, 150, 300 or 600 μg/mL to make the final concentration of 37.5, 75, 150 or 300 μg/mL. The MMC drug-free NPs and RBCs were vortexed briefly, left at 37 °C for 60 min, then centrifuged at 10, 000 rpm for 5 min. The supernatant was transferred to a plate and the absorbance value of hemoglobin at 577 nm was determined with a reference wavelength of 655 nm. The same volume of PBS was used as the negative control, and water was the positive control. The percentage of hemolysis was calculated by the formula as previously reported. [28] The results were included in Fig. S4†.

In vivo pharmacokinetics

All the animal procedures complied with the guidelines of the Xiamen University Institutional Animal Care and Use Committee. The experiments were performed on adult male SD rat weighing 200 ± 20 g (mean ± SD) from Shanghai Laboratory Animal Center. To evaluate the circulation half-life of the MTX-PEG-PE-PLA NPs/MMC-SPC, the MTX-PEG-PE-PLA NPs/MMC-SPC at 4 mg/kg (MMC-eq. dose) were injected into the tail vein of the rat. Three hundred microliters of blood were collected into heparinized tubes at 1, 5, 15, 30 min, and 1, 2, 4, 8, 12, 24 and 48 h following the injection. The heparinized blood samples were centrifuged immediately at 3, 000 rpm for 15 min at 4 ℃ to harvest the plasma and stored at -80 ℃ until

analysis. MMC were extracted from the plasma by deproteinization using ethyl acetate followed by centrifugation at 12, 000 rpm for 10 min. The PEG-PE-PLA NPs/MMC-SPC and free MMC at MMC-eq. dose were also tested in parallel as controls. Each group contained six rats. The plasma MMC concentrations were determined by LC-MS/MS method with 4-aminoacetophenone as internal standard. The chromatographic separations were acquired on a Waters Acquity HPLC system (Waters Corporation, Milford, MA, USA) equipped with a Waters e2695 separations module, a Waters 2998 photodiode array detector and a Hypersil GOLD C_{18} column. HPLC grade acetonitrile/water (25/75, v/v) was used as the mobile phase. The compounds were analyzed by multiple reaction monitoring of the transitions of m/z 335→242 for MMC and m/z 136→94 for 4-aminoacetophenone, respectively. The pharmacokinetic parameters such as elimination half-life ($t_{1/2}$), area under the curve (AUC), volume of distribution (Vd) and clearance (CL) were calculated by fitting the blood drug pharmaceutical concentrations to a two-compartment model using WinNonlin Professional Edition Version 2.1 (Pharsight Corporation, Mountain View, California).

Cell culture

HeLa cells or Caco-2 cells were cultured in FA-deficient Dulbecco's Modified Eagle's Medium (DMEM) supplemented with 10% fetal bovine serum (FBS) and 1% penicillin-streptomycin. A549 cells or MC 3T3-E1 cells were respectively cultured in FA-deficient Roswell Park Memorial Institute (RPMI) 1640 medium or Minimum

Essential Medium, Alpha Modified (α-MEM) under similar conditions. The four cell lines have different levels of FA receptor expression. In particular HeLa cells and Caco-2 cells are FA receptor positive, and A549 cells and MC 3T3-E1 cells are FA receptor negative. All of the cells were cultivated in a humidified atmosphere containing 5% CO_2 at 37 ºC.

In vitro cellular uptake

To facilitate the observation of cellular uptake, the hydrophobic red fluorescent DiD were added to the oil phase and encapsulated into the MTX-PEG-PE-PLA NPs/MMC-SPC. HeLa cells, A549 cells, Caco-2 cells or MC 3T3-E1 cells were seeded at a density of 8×10^4 cells per well in 6-well plates with their specific cell culture medium. The cells were incubated at 37 °C and 5% CO_2 for 24 h. 100 μL of the MTX-PEG-PE-PLA NPs/MMC-SPC/DiD or PEG-PE-PLA NPs/MMC-SPC/DiD (1 mg/mL) at DiD-eq. dose was added and incubated further for 6 h. The cells were washed with PBS, fixed with 4% paraformaldehyde and stained with Hoechst 33258. The cells were observed using a Leica TCS SP5 LCSM (Leica Microsystems, Mannheim, Germany).

Additionally, to investigate the competitive inhibition effect for easier observation, HeLa cells were pre-incubated in a cell culture medium supplemented with the free FA (1 mg/mL) for 30 min prior to adding the MTX-PEG-PE-PLA NPs/MMC-SPC/DiD.

Flow cytometery

To quantitatively measure the internalization of these NPs, HeLa cells were incubated in 6-well plates (2 mL of cell suspension per well) at a density of 1×10^5 cells/mL, then cultured with the DiD-PEG-PE-PLA NPs/MMC-SPC or DiD-MTX-PEG-PE-PLA NPs/MMC-SPC at DiD-eq. dose as described above. After incubation for the predesigned time, the cells were washed with cold PBS, harvested by 0.25% Trypsin-EDTA, centrifuged at 1, 000 rpm for 5 min at 4 °C and resuspended in PBS. The fluorescence intensity of the cells was conducted using a Beckman Coulter EPICS XL flow cytometer (Beckman Coulter, CA, USA) and data analyzed with CellQuest software (Becton-Dickinson, San Jose, CA, USA).

In vitro cell viability

The cytotoxicity of the MTX-PEG-PE-PLA NPs/MMC-SPC was evaluated by CCK-8 assay. HeLa cells and A549 cells were seeded at a density of 1×10^4 cells per well in 96-well plates, pre-incubated for 24 h, and then incubated with the MTX-PEG-PE-PLA NPs/MMC-SPC for 24 or 72 h. The MTX-PEG-PE-PLA NPs/MMC-SPC with MMC dose ranged from 3 to 12 μg/mL. After incubation for 24 or 72 h, 20 μL of CCK-8 was added and incubated for further 2 h. Absorbance at 450 nm was measured using a Bio-Rad Model 680 microplate reader (Richmond, CA, USA). The cells treated with the free MMC or PEG-PE-PLA NPs/MMC-SPC were used as controls. The cytotoxicity of the PEG-PE-PLA NPs/SPC and MTX-PEG-PE-PLA NPs/SPC was also tested as the method above, and the dose of the NPs varied from 37.5 to 300 μg/mL.

Intracellular delivery

HeLa cells were seeded, incubated at 37 °C for 24 h, and then cultured with the MTX-PEG-PE-PLA NPs/MMC-SPC/DiD at 37 °C for 8 h. The cells were imaged using a LCSM. Lysotracker green was used to stain late endosomes and lysosomes. Hoechst 33258 was used to stain nuclei.

Additionally, to understand the intracellular distribution of the MMC drug, the FITC-MMC was prepared for use as a fluorescent probe. [29] HeLa cells were seeded, incubated at 37 °C for 12 h, and then cultured with the MTX-PEG-PE-PLA NPs/FITC-MMC-SPC/DiD at 37 °C for 12 h. Hoechst 33258 was used to stain nuclei.

Ex vivo tumor targeted imaging

Female BALB/c nude mice aged 5 weeks (16-20 g) were supplied by Shanghai Laboratory Animal Center and kept under specific pathogen-free conditions with free access to standard food and water. The tumor model was established by inoculating 1 $\times 10^6$ H_{22} cells in the right axillary region of each nude mouse.

DiR, a near-infrared fluorescent probe, was encapsulated into the NPs. The MTX-PEG-PE-PLA NPs/MMC-SPC/DiR were prepared using the procedures described above. To investigate the tumor targeting efficiency of the NPs on the H_{22} tumor-bearing nude mice, when the tumor volumes reached a predetermined size range, 0.2 mL of the MTX-PEG-PE-PLA NPs/MMC-SPC/DiR were injected into the mice via the tail vein. At 12 h post-injection, the mice were sacrificed. The tumor and

major organs (heart, spleen, lung, kidney and liver) were excised, followed by washing the surface with 0.9% NaCl for the ex vivo imaging of DiR fluorescence using a Maestro^{TM} in vivo imaging system (Cambridge Research & Instrumentation, Woburn, MA, USA). The mice treated with 0.2 mL of the PEG-PE-PLA NPs/MMC-SPC/DiR at DiR-eq. dose were used for comparison. To investigate the detail of DiR distribution at the tumor site, the removed tumors were fixed with neutral paraformaldehyde, embedded into paraffin, sectioned and observed using LCSM at the exact same settings.

In vivo biodistribution

To assess the biodistribution of MMC formulations, the H_{22} tumor-bearing mice were intravenously injected via tail vein with the PEG-PE-PLA NPs/MMC-SPC or MTX-PEG-PE-PLA NPs/MMC-SPC at MMC-eq. dose. The mice were sacrificed at the predesigned times after administration, and the heart, spleen, lung, kidney, liver and tumor were excised and washed with cold 0.9% NaCl. Tissue samples were then homogenized and mixed with the mixture of acetonitrile/water (25/75, v/v). MMC was extracted using ethyl acetate followed by centrifugation at 12, 000 rpm at 4 °C for 10 min. The MMC content in supernatant was then measured by a HPLC method described above and expressed as percentage of the injected dose pergram of tissue (% ID/g tissue).**In vivo anticancer effect**

Kunming mice aged 4-5 weeks (clean class, 18-22 g) were supplied by Xiamen University Laboratory Animal Center and used in this study. Subcutaneous tumors

were established in the mice by subcutaneous inoculation of H_{22} cells in the right axillary region of mice before the treatment. After the tumor implantation for one week, the H_{22} tumor bearing mice were randomly divided into 4 groups (10 mice per group): group 1 for 0.9% NaCl, group 2 for MMC injection, group 3 for PEG-PE-PLA NPs/MMC-SPC, group 4 for MTX-PEG-PE-PLA NPs/MMC-SPC. The mice were intravenously injected at 4 mg/kg (MMC-eq. dose) every two days for 3 times. Each mouse was earmarked and followed individually throughout the whole experiments. The width and length of the tumors and the body weight of mice were measured every two days until the animals were terminated. Tumor volume (V) was calculated by the formula as previously reported. [12] The mice were terminated on day 15. The tumors were excised and then weighed. The tumor growth inhibition rate was calculated by the formula as previously reported. [30] For histological examination, the tumors harvested from all 4 groups were fixed in 10% buffered formalin, embedded in paraffin, sectioned, stained with hematoxylin & eosin (H&E) and examined using a digital microscopy system.

Statistical analysis

All experiments were performed at least three times. All data were expressed as mean ± SD. The two-tailed Student's *t*-test for two groups was performed to evaluate the statistical significance. The statistical difference was considered to be significant when the P value was less than 0.05.

Results and discussion

Preparation of MTX-PEG-PE-PLA NPs/MMC-SPC

The procedure for synthesizing DSPE-PEG-MTX by a PEGylated lipid-drug conjugation approach is schematically illustrated in Fig. 1A. ^{1}H NMR spectrum of DSPE-PEG-MTX (Fig. 1B) presented the peaks at 8.6, 7.7 and 6.8 ppm, which were assigned to the protons of the pteridine ring and p-phenyl ring of MTX. UV-Vis spectrum of DSPE-PEG-MTX (Fig. 1C) displayed the peaks at 258 and 305 nm derived from the structure of MTX. [31] All of the results were suggestive of the synthesis of DSPE-PEG-MTX.

In this paper, given the popularity of PLA NPs as model drug carriers, the efficient encapsulation of MMC as a water-soluble small molecular drug into hydrophobic PLA using traditional methods may be a challenge. To overcome the great challenge, we introduced the lipid-drug complex approach into the PLA-PE-PEG NPs to improve the encapsulation efficiency as well as control the drug release. The MTX-PEG-PE-PLA NPs/MMC-SPC drug delivery system was schematically illustrated in Fig. 2A (more details were shown in Fig. S1†). The biocompatible and biodegradable PLA was used to encapsulate and stabilize the MMC-SPC complex. In the first W/O emulsion, the fat-soluble tail of SPC was outward to the PLA oil phase, and MMC was protected inward to the internal water phase. In the double W/O/W emulsion, DPPE, DSPE-PEG and DSPE-PEG-MTX were adsorbed and self-assembled at the oil-water interface by hydrophobic-hydrophobic interactions with their hydrophobic tail groups oriented toward the PLA oil phase. Through the double emulsion process, the MTX-PEG-PE-PLA NPs/MMC-SPC were prepared.

More notably, DSPE-PEG-MTX was not only used as a structural element of the PLA-PE-PEG NPs, but also served as a targeting ligand to rapidly target the PLA-PE-PEG NPs to the site of interest.

The particle size of the MTX-PEG-PE-PLA NPs/MMC-SPC increased and the zeta potential of those decreased with increasing weight ratio of MMC-SPC to PLA (Fig. S2A†). We presented a model of the distribution of drug-phospholipid complex in the MTX-PEG-PE-PLA NPs/MMC-SPC drug delivery system (Fig. S2B†). When the ratio of MMC-SPC to PLA is low, all of MMC-SPC distributed at the interface of the inner water-oil with their lipophilic parts oriented toward the PLA oil phase. When the ratio is high, the residual MMC-SPC was transported to the interface of the oil-outer water with their hydrophilic parts oriented toward the external water phase. Moreover, the excess of MMC-SPC might participate in the self-organization of the phytosomes (typical particle size is about 50-500 nm) or large size, vesicle-like structures. [15,32] We thus pursed an optimization by using a MMC-SPC/PLA ratio of 20% to prepare the MTX-PEG-PE-PLA NPs/MMC-SPC.

Particle size, PDI, zeta potential and morphology

The NPs of a size of 40-400 nm can be passively accumulated at the tumor site from the leaky tumor vasculature with the poor lymphatic drainage. [33,34] The zeta potential was a great indication for in vitro and in vivo stability of the NPs. [11] The MTX-PEG-PE-PLA NPs/MMC-SPC presented a spherical shape (Fig. 2C and 2D) and a small particle size (219.6 ± 2.1 nm) with a narrow particle size distribution (Fig.

2E), which might therefore be favorable for operating EPR effect. The MTX-PEG-PE-PLA NPs/MMC-SPC with a zeta potential of -24.76 ± 2.71 mV (Fig. 2F) indicated their extra electrostatic stability at physiological pH. In addition, the coexistence of $-COO^-$ and $-NH_3^+$ as "zwitterions" was an important structural feature of the NPs since it could weaken the rapid RES clearance and facilitate the passive cell uptake for in vivo use. [35]

In vitro stability tests

A short-term stability test. The variation in the particle size of the drug delivery systems was a vital index to evaluate their stability in PBS or plasma. No significant particle size change of the NPs in PBS or 10% plasma was observed even after 120 h (Fig. S3A†). The result indicated the effective physiological stability against ionic strength and protein adsorption owing to the electrostatic repulsion, steric repulsion and structural longevity of the NPs. Once intravenously administrated, the NPs had potential to promote the blood persistence.

A long-term stability test. The lyophilization technique was adopted as a pivotal step for a long-term storage of the drug delivery systems in the pharmaceutical industry. The lyophilized MTX-PEG-PE-PLA NPs/MMC-SPC could be re-dispersed in DI water, similar to the freshly prepared NPs. No significant change of the particle size, zeta potential and encapsulation efficiency was also shown in the lyophilized NPs (Fig. S3B†) at 4 or 25 °C in 3 months. The result indicated that the polymer-lipid hybrid NPs and drug-phospholipid complex could protect the drug against rapid degradation.

In vitro drug release

The drug release of the MTX-PEG-PE-PLA NPs/MMC-SPC was performed in a dialysis bag. In sharp contrast to the free MMC, a prolonged release was observed for the PEG-PE-PLA NPs/MMC-SPC and MTX-PEG-PE-PLA NPs/MMC-SPC (Fig. 3A). Outperformed the free drug, a sustained drug transport of the drug-loaded PEG-PE-PLA NPs was predominantly driven by a diffusion-controlled mechanism: at first, MMC was dissociated from the complex uniformly and effectively dispersed within the internal core, and then the free MMC diffused through the skeleton of the polymer-lipid hybrid NPs. A long-acting effect of the MTX-PEG-PE-PLA NPs/MMC-SPC on drug release indicated that these MTX-PEG-PE-PLA NPs/MMC-SPC were expected to be long-lasting and effective MMC delivery systems.

Besides, the encapsulation efficiency of the MTX-PEG-PE-PLA NPs/MMC-SPC (90.5 ± 3.0%) was higher than that of the MTX-PEG-PE-PLA NPs/MMC+SPC (76.0 ± 3.1%) or MTX-PEG-PE-PLA NPs/MMC (51.8 ± 3.9%), we hypothesized that the MMC-SPC complex may prevent the drug diffusion outwards during the NPs preparation, leading to little drug released or destroyed. To test the hypothesis, we investigated the MMC release profile with different interaction between MMC and SPC (MMC-SPC, MMC+SPC, MMC without SPC) in the MTX-PEG-PE-PLA NPs (Fig. 3B), the even more gradual and stepwise drug release from the MTX-PEG-PE-PLA NPs/MMC-SPC can be understood in terms of the molecular restriction of the lipid-drug complex. The strong physical interaction between

MMC-SPC complex played a vital role against both water penetration and drug diffusion. Therefore, the introduction of the lipid-drug complex not only increased the drug encapsulation efficacy but also blocked the drug release. Furthermore, the well-encapsulated efficiency and the prolonged drug release could prevent the side effects to normal cells.

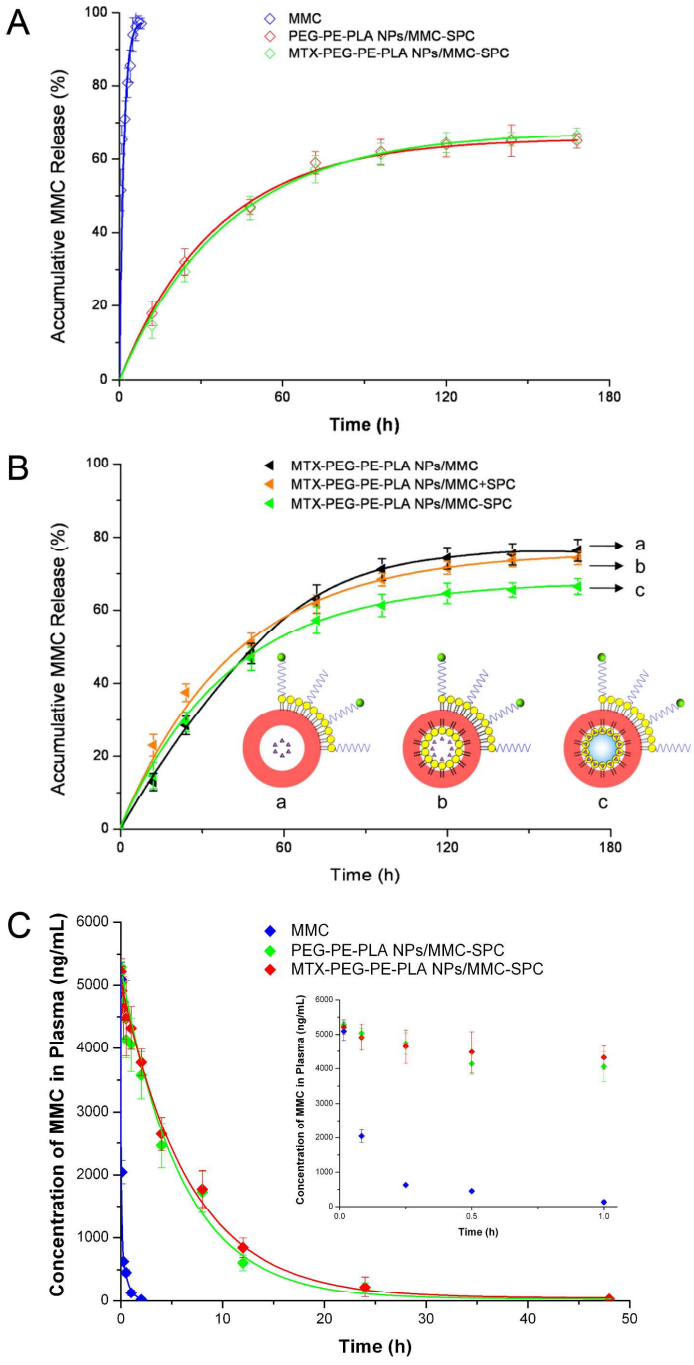

Fig. 3 (A) In vitro release profiles of MMC in PBS (pH 7.4) from the free MMC, PEG-PE-PLA NPs/MMC-SPC and MTX-PEG-PE-PLA NPs/MMC-SPC (mean ± SD, n = 3). (B) In vitro release profiles of MMC in PBS (pH 7.4) from the (a) MTX-PEG-PE-PLA NPs/MMC, (b) MTX-PEG-PE-PLA NPs/MMC+SPC, (c) MTX-PEG-PE-PLA NPs/MMC-SPC (mean ± SD, n = 3). (C)

In vivo pharmacokinetics of MMC in rats after intravenous administration of the free MMC, PEG-PE-PLA NPs/MMC-SPC and MTX-PEG-PE-PLA NPs/MMC-SPC. (mean ± SD, n = 6).

In vivo pharmacokinetics

No notable hemolytic effects for hemolysis analysis were observed even at the highest NPs dose of 300 μg/mL in PBS (Fig. S4†), this is a proof to confirm that the PEG-PE-PLA NPs/SPC or MTX-PEG-PE-PLA NPs/SPC possessed a good blood compatibility (<2% hemolysis). [36]

To investigate in vivo pharmacokinetic of MMC, SD rat was treated with a single intravenous injection of the MMC injection, PEG-PE-PLA-NPs/MMC-SPC or MTX-PEG-PE-PLA NPs/MMC-SPC at 4 mg/kg (MMC-eq. dose). Plasma MMC concentration was the highest at the completion of injection and gradually decreased thereafter (Fig. 3C). As shown in the blood clearance curves (Fig. 3C) and the pharmacokinetic parameters using a two-compartment model (Table 1), we can find that the blood circulation time of both PEG-PE-PLA-NPs/MMC-SPC and MTX-PEG-PE-PLA NPs/MMC-SPC was similar but significantly extended compared to the free MMC, with a significantly longer elimination half-life ($t_{1/2}$), a remarkably higher area under the curve (AUC) and a substantially lower value for clearance (CL). The result might be explained by the in vitro controlled/sustained drug release based on the hybrid NPs structure and in vivo extended circulation based on the PEGylated nanoscaled delivery systems.

Table 1. Pharmacokinetic parameters of MMC in mice after intravenous administration of the free MMC,

PEG-PE-PLA NPs/MMC-SPC and MTX-PEG-PE-PLA NPs/MMC-SPC at dose of 4 mg/kg (mean ± SD, n = 6).

	$t_{1/2}$ (h)	CL (L/h/kg)	AUC (μg/L*h)	V_d (L)
MMC	0.35±0.02	4.40±0.49	916.1±101.3	2.19±0.16
PEG-PE-PLA NPs/MMC-SPC	6.36±0.68[a]	0.11±0.02	35541.1±5386.8	1.05±0.19
MTX-PEG-PE-PLA NPs/MMC-SPC	6.66±1.00[a,b]	0.10±0.02	38972.2±7465.7	0.99±0.04

[a] $P < 0.05$ vs MMC. [b] $P > 0.05$ vs PEG-PE-PLA NPs/MMC-SPC.

In vitro cellular uptake

The targeting ability of the MTX-PEG-PE-PLA NPs/MMC-SPC to FA receptor-overexpressed cancer cells was studied using HeLa cells as an example. To investigate the cell uptake of the PEG-PE-PLA NPs/MMC-SPC and MTX-PEG-PE-PLA NPs/MMC-SPC in HeLa cells by LCSM, we loaded red fluorescent DiD into the PEG-PE-PLA NPs/MMC-SPC and MTX-PEG-PE-PLA NPs/MMC-SPC. The cellular uptake of the MTX-PEG-PE-PLA NPs/MMC-SPC/DiD increased than that of the PEG-PE-PLA NPs/MMC-SPC/DiD at DiD-eq. dose (Fig. 4Aa and 4Ab). To address the selectivity of the MTX-PEG-PE-PLA NPs/MMC-SPC for FA receptors, we performed a competition assay. HeLa cells were pretreated with an excess of the free FA, followed by incubation with the MTX-PEG-PE-PLA NPs/MMC-SPC/DiD, the enhanced intracellular internalization of NPs was greatly

inhibited (Fig. 4Ac). On the other hand, the difference of the cellular uptake of the MTX-PEG-PE-PLA NPs/MMC-SPC/DiD towards HeLa cells (FA receptor positive) and A549 cells (FA receptor negative) was significant (Fig. 4Ab and 4Ad), and the difference of the cellular uptake of those towards Caco-2 cells (FA receptor positive) and MC 3T3-E1 cells (FA receptor negative) was also significant (Fig. S5A†). These results gave us a strong evidence that the use of MTX offered a selective targeting efficiency. The high selectivity (as illustrated in Fig. S5B†) might widen their usage as an ideal candidate for therapeutic drug delivery with expected targeting effect and reduced side effect.

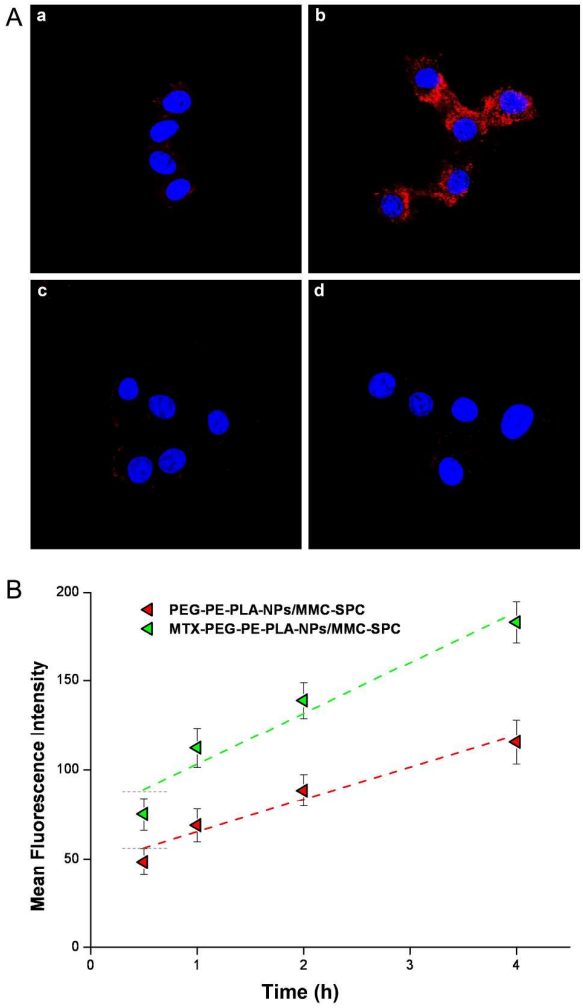

Fig. 4 (A) Qualitative cellular uptake analysis of the MTX-PEG-PE-PLA NPs/MMC-SPC. HeLa cells were FA receptor-positive and A549 cells were FA receptor-negative. (a) HeLa cells were treated with the PEG-PE-PLA NPs/MMC-SPC/DiD. (b) HeLa cells were treated with the MTX-PEG-PE-PLA NPs/MMC-SPC/DiD. (c) HeLa cells were blocked with the free FA and then treated with the MTX-PEG-PE-PLA NPs/MMC-SPC/DiD. (d) A549 cells were treated with the MTX-PEG-PE-PLA NPs/MMC-SPC/DiD. The DiD-loaded NPs/MMC-SPC appeared in red. (B) Quantitative cellular uptake analysis of the MTX-PEG-PE-PLA NPs/MMC-SPC. Flow cytometery of the PEG-PE-PLA NPs/MMC-SPC/DiD and MTX-PEG-PE-PLA NPs/MMC-SPC/DiD under 0.5, 1, 2 and 4 h treatment (mean ± SD, n = 3).

Flow cytometery

To confirm the targeting efficiency of the MTX-PEG-PE-PLA NPs/MMC-SPC, the quantitative analysis of the cellular uptake was performed by flow cytometery. The intracellular fluorescence intensity increased as the incubation time was extended from 0.5 to 4 h (Fig. 4B). The MTX-PEG-PE-PLA NPs/MMC-SPC/DiD exhibited the higher cellular uptake efficiency compared with the PEG-PE-PLA NPs/MMC-SPC/DiD at DiD-eq. dose, indicating that MTX improved the targeting efficacy. The difference of cellular uptake can be explained by their distinct endocytosis mechanisms. On the one hand, the lipophilicity of lipid possessing a similar structure component with phospholipids of the cell membranes perhaps promoted the endocytosis and hence facilitated the passive delivery of the PEG-PE-PLA NPs/MMC-SPC/DiD to the interior of the cells. [15,37,38] On the other hand, the cellular uptake of the MTX-PEG-PE-PLA NPs/MMC-SPC/DiD was further

increased via a selective ligand-receptor interaction. The quantitative result was in good agreement with the qualitative result, giving a further proof of the improved cellular uptake efficiency of the MTX-PEG-PE-PLA NPs/MMC-SPC.

In vitro cell viability

It is important to deliver sufficient amounts of anticancer drugs to the target cells. After incubating HeLa cells with the MTX-PEG-PE-PLA NPs/FITC-MMC-SPC compared to the PEG-PE-PLA NPs/FITC-MMC-SPC, higher accumulation of FITC-MMC in the nuclei of HeLa cells was shown in Fig. S6A† Thus, the targeting efficacy of the MTX-PEG-PE-PLA NPs/MMC-SPC offered the great potential to effectively kill HeLa cells.

To evaluate the cytotoxicity of the MTX-PEG-PE-PLA NPs/MMC-SPC, we chose two cancer cell lines: HeLa cells (high levels of FA receptor expression) and A549 cells (low levels of FA receptor expression). No significant adverse effect against HeLa cells or A549 cells was demonstrated in the PEG-PE-PLA NPs as well as the MTX-PEG-PE-PLA NPs (Fig. S6B†). These results indicated that the MMC drug-free PEG-PE-PLA NPs as well as the MTX-PEG-PE-PLA NPs had little toxicity to both HeLa cells and A549 cells at the concentration from 37.5 to 300 μg/mL.

Next, we used these two cell lines to assess the efficacy of the targeting ligand MTX. On the one hand, the MTX-PEG-PE-PLA NPs/MMC-SPC and PEG-PE-PLA NPs/MMC-SPC presented a dose-dependent cytotoxicity against HeLa cells (Fig. 5A) or A549 cells (Fig. S6C†). On the other hand, the MTX-PEG-PE-PLA NPs/MMC-SPC induced a more potent cytotoxicity over the PEG-PE-PLA

NPs/MMC-SPC against HeLa cells, but not against A549 cells. Such a dramatic difference in cytotoxicity revealed that the successful targeting effect of MTX could play a key role in the selectively enhanced cytotoxic effects.

After incubation for 24 h, the cytotoxicities of the PEG-PE-PLA NPs/MMC-SPC and MTX-PEG-PE-PLA NPs/MMC-SPC against HeLa cell were not as effective as the free MMC (Fig. 5A). In contrast, after incubation for 72 h, the cytotoxicities of HeLa cells with the treatment of the PEG-PE-PLA NPs/MMC-SPC and MTX-PEG-PE-PLA NPs/MMC-SPC were significantly higher than the treatment of the free MMC (Fig. 5B). Notably, the highest cell cytotoxicity appeared at the highest concentration of the NPs formulation after the longest treatment time indicated that the anticancer drugs were released from the drug delivery systems in a sustained/controlled manner over a long period of time for an improved effect.

The results can be ascribed to the improved targeting efficacy of MTX, the enhanced cellular internalization of the NPs size effect as well as the sustained/controlled drug release of the nanoscaled drug delivery systems, which lead to the cytotoxicity enhancement effect of anticancer drug. All of the results suggested that the FA receptor-mediated endocytosis and sustained/controlled drug release could efficiently lead to the progressive increase of intracellular drug level for cell apoptosis/death compared with the passive diffusion of the free MMC without drug release.

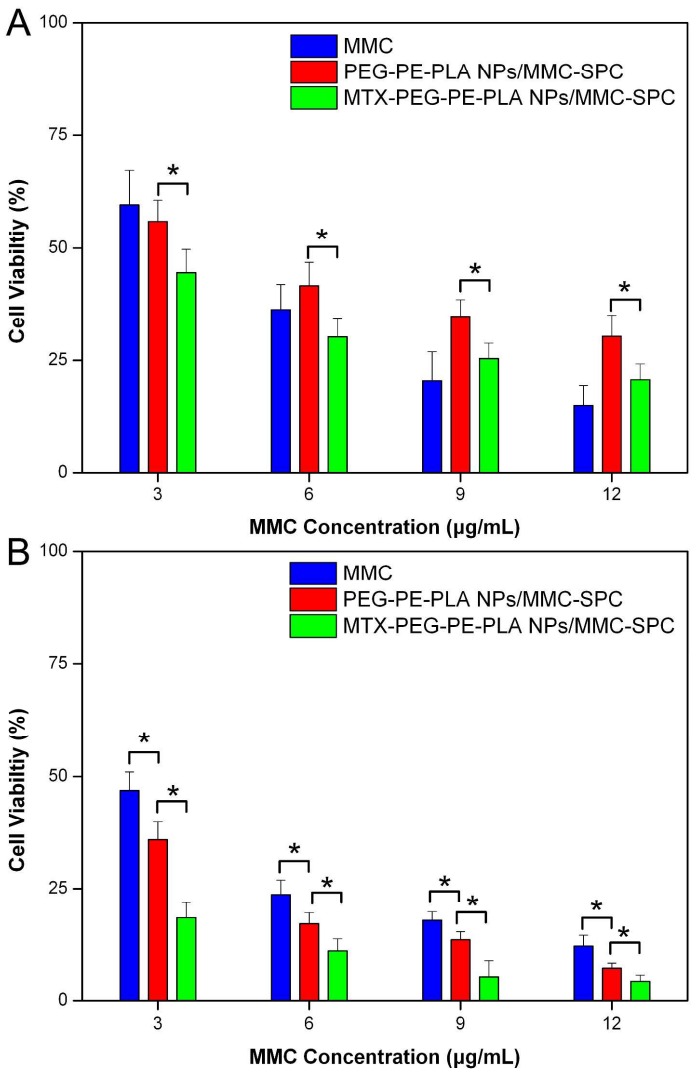

Fig. 5 Cell viability of the MTX-PEG-PE-PLA NPs/MMC-SPC. HeLa cells were incubated with the free MMC, PEG-PE-PLA NPs/MMC-SPC and MTX-PEG-PE-PLA NPs/MMC-SPC after incubation for (A) 24 and (B) 72 h (mean ± SD, n = 6). * $P < 0.05$.

Versatile therapeutic drug delivery

To investigate the state of the MTX-PEG-PE-PLA NPs/MMC-SPC in a buffer environment at different pH values, the NPs were immersed in PBS (pH = 7.4, 6.5 or 5.5) for 4 h. The particle size of the NPs increased as pH decreased (Fig. 6A). As pH decreased from 7.4, via 6.5 (DPPE was partly protonated but the intra- or

inter-molecular hydrophobic interactions of the NPs was still strong) to 5.5, the NPs were disintegrated and aggregated into larger formation. [39,40] These results also indicated that the NPs might be stable at the tumor pH and would disintegrate at endo/lysosomal pH.

Additionally, the drug release behavior of the MTX-PEG-PE-PLA NPs/MMC-SPC was strongly dependent on the pH value of PBS (Fig. 6B). In agreement with the previous reports, [41-43] these results indicated that phosphatidylethanolamine was pH-sensitive, which was favorable for achieving a controlled drug release in cancer cells. [44,45] Once the MTX-PEG-PE-PLA NPs/MMC-SPC are intravenously administered, the drug protection is maximized and the systemic toxicity is minimized.

To investigate the intracellular delivery of the MTX-PEG-PE-PLA NPs/MMC-SPC, HeLa cells were treated with the MTX-PEG-PE-PLA NPs/MMC-SPC/DiD. Some red fluorescent signals resided in the green fluorescent endo/lysosomes, indicating that the NPs were internalized into the endo/lysosomes via the endocytosis pathway (Fig. S7A†). [30] A part of the NPs were no longer located in the endo/lysosomes, owing to the proton absorbing activity of -NH_2 group of PE lipid moiety inside the endo/lysosomes. [35,39] The result was also similar to the reported work, [30] indicating the endo/lysosomal escape of the NPs.

To this end, as illustrated in Fig. 6C, once the nanoscaled drug delivery systems reached to the target site, there would be a rapid cellular internalization (see Fig. 4A and 4B), efficient endo/lysosomal escape (see Fig. S7A†) and a sustained/controlled

drug release (see Fig. 3A, 3B and 6B), resulting in the enhanced internalization and accumulation of drug in the nuclei (Fig. S7B†). All of these results could also contribute to increasing the anticancer activity the MTX-PEG-PE-PLA NPs/MMC-SPC (see Fig. 5).

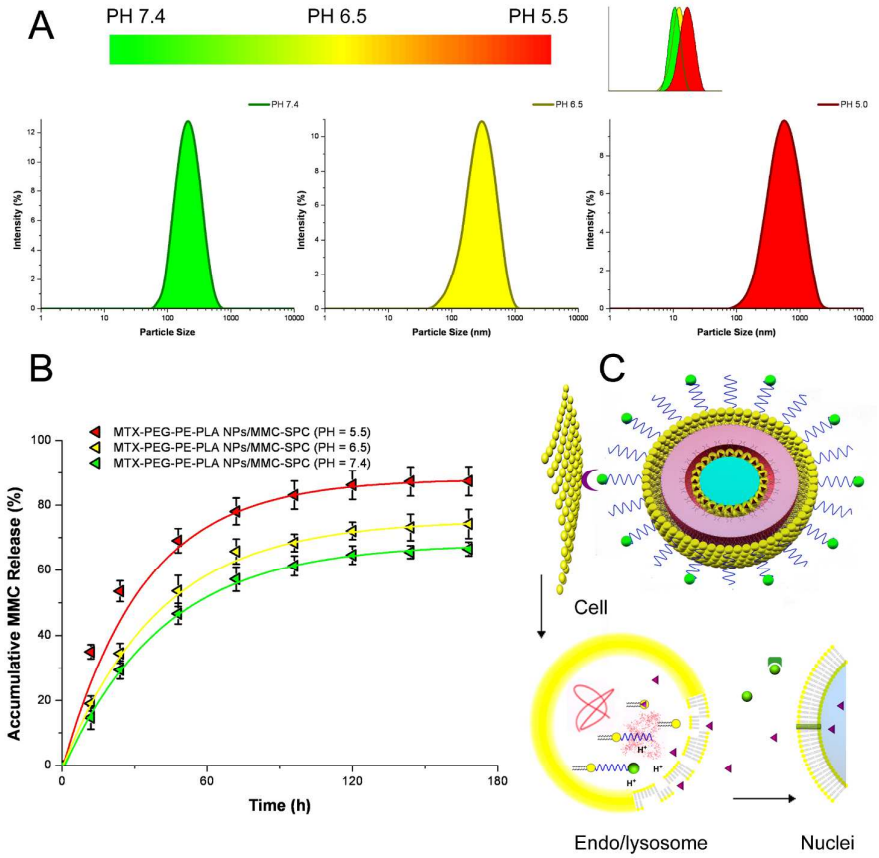

Fig. 6 pH-dependent MMC release of the MTX-PEG-PE-PLA NPs/MMC-SPC. (A) Particle size of the MTX-PEG-PE-PLA NPs/MMC-SPC in PBS (pH 7.4, 6.5 and 5.5) under 4 h incubation. (B) In vitro release profiles of MMC from the MTX-PEG-PE-PLA NPs/MMC-SPC in PBS (pH 7.4, 6.5 and 5.5) (mean ± SD, n = 3). (C) Illustrations of versatile therapeutic drug delivery: the selective cell uptake, endo/lysosome escape and controlled/sustained release.

Ex vivo tumor targeting imaging

The in vitro study demonstrated the targeting effect of the MTX-PEG-PE-PLA/MMC-SPC to HeLa cells, which motivated us to further investigate their in vivo performance. Murine hepatoma H_{22} tumor with overexpressed FA receptors was transplanted into the mice before the in vivo study. [46-48] To evaluate the tumor targeting efficacy of the MTX-PEG-PE-PLA NPs/MMC-SPC in vivo, we loaded red fluorescent DiR into the drug delivery systems. The MTX-PEG-PE-PLA NPs/MMC-SPC/DiR and PEG-PE-PLA NPs/MMC-SPC/DiR were injected intravenously into nude mice bearing H_{22} tumors at DiR-eq. dose. As clearly shown in Fig. 7A and 7B, some PEG-PE-PLA NPs/MMC-SPC/DiR accumulated in the tumor, but much more was enriched in the liver. On the contrary, much MTX-PEG-PE-PLA NPs/MMC-SPC/DiR accumulated in the tumor compared to the normal organs. More importantly, compared to the PEG-PE-PLA NPs/MMC-SPC/DiR group, the MTX-PEG-PE-PLA NPs/MMC-SPC/DiR group exhibited the significantly higher fluorescence intensity in tumor and lower fluorescence intensity in normal organs. These results indicated the less RES uptake and higher tumor accumulation of the MTX-PEG-PE-PLA NPs/MMC-SPC over the PEG-PE-PLA NPs/MMC-SPC. [49] Further observation of the tumor sections by LCSM (Fig. 7C) proved the ex vivo fluorescent image and data. All results suggested that the MTX-PEG-PE-PLA NPs/MMC-SPC possessed high tumor targeting efficiency.

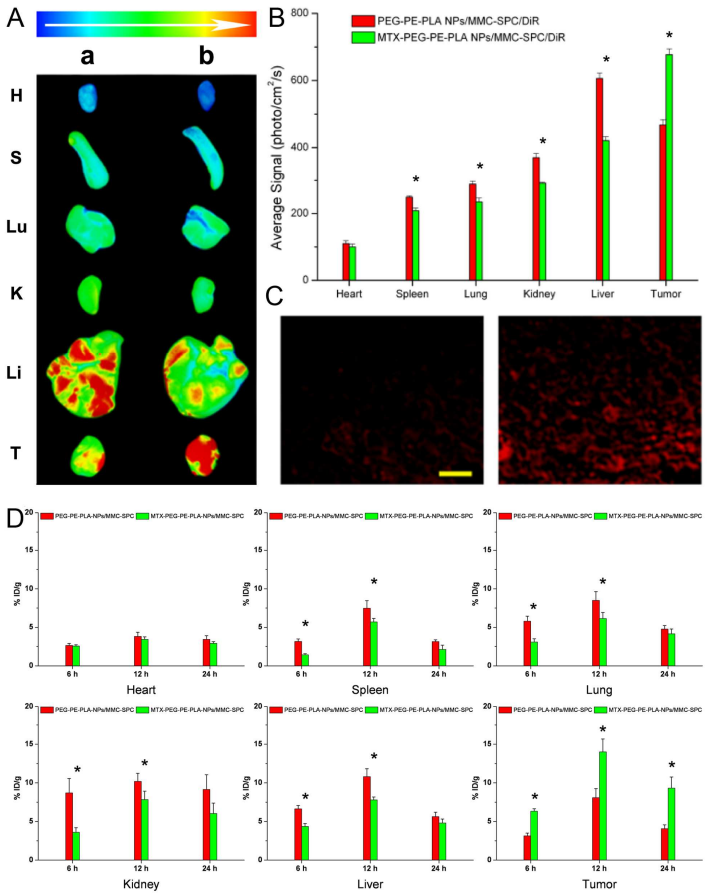

Fig. 7 In vivo tumor targeted imaging and biodistribution of the MTX-PEG-PE-PLA NPs/MMC-SPC. (A) Ex vivo fluorescence imaging of normal organs and tumor excised from H_{22} tumor-bearing mice treated with the (a) PEG-PE-PLA NPs/MMC-SPC/DiR or (b) MTX-PEG-PE-PLA NPs/MMC-SPC/DiR at 12 h post-injection. (B) Quantitative tumor target characteristics of the PEG-PE-PLA NPs/MMC-SPC/DiR and MTX-PEG-PE-PLA NPs/MMC-SPC/DiR (mean ± SD, n = 3). Statistical significance compared with the PEG-PE-PLA/MMC-SPC/DiR group: * $P < 0.05$. (C) Ex vivo distribution in the tumor sections from H_{22} tumor-bearing mice treated with the (a) PEG-PE-PLA NPs/MMC-SPC/DiR or (b) MTX-PEG-PE-PLA NPs/MMC-SPC/DiR. Scale bar = 20 μ m. (D) Quantitative analysis for tissue distribution of MMC in H_{22} tumor-bearing mice treated with the PEG-PE-PLA/MMC-SPC or MTX-PEG-PE-PLA/MMC-SPC (mean ± SD, n = 4). Statistical

significance compared with the PEG-PE-PLA/MMC-SPC group:, * $P < 0.05$.

In vivo biodistribution

To assess the MMC biodistribution in mice, the MTX-PEG-PE-PLA NPs/MMC-SPC was intravenously injected into mice bearing H_{22} tumors via their tail vein. As shown in Fig. 7D, compared to the PEG-PE-PLA NPs/MMC-SPC group, the MTX-PEG-PE-PLA NPs/MMC-SPC group demonstrated the increased MMC accumulation in the tumor at 12 h post-injection, just because the targeting ligand-MTX can specifically bind their receptors in the tumor cells and enhance the cellular uptake of the MTX-PEG-PE-PLA NPs/MMC-SPC. Longer exposure to MMC with the effective therapeutic level was also a prerequisite for a greater therapeutic efficacy. Besides, the less MMC drug accumulation in the normal organs was observed for the MTX-PEG-PE-PLA NPs/MMC-SPC compared to the PEG-PE-PLA NPs/MMC-SPC at 12 h post-injection. The result gave a further support of the less RES uptake and more tumor accumulation of the MTX-PEG-PE-PLA NPs/MMC-SPC over the PEG-PE-PLA NPs/MMC-SPC. All of the imaging and biodistribution results suggested that with the assistance of the EPR effect and the long circulation effect, the specific targeting effect of MTX-PEG-PE-PLA NPs/MMC-SPC can further improve the accumulation of the MMC drug delivery systems at the tumor site.

In vivo anticancer effects

To verify whether the tumors in the mice were inhibited by the

MTX-PEG-PE-PLA NPs/MMC-SPC, the in vivo anticancer effect was tested using a H_{22} tumor model. It was encouraging to find that the tumor growth of mice treated with the MTX-PEG-PE-PLA NPs/MMC-SPC was slower than that of mice treated with PEG-PE-PLA NPs/MMC-SPC and free MMC, and this difference became more significant ($P < 0.05$) after day 15 (Fig. 8A). At the end of experiment, the tumor growth inhibition rate of the MTX-PEG-PE-PLA NPs/MMC-SPC group was also significantly higher compared to the PEG-PE-PLA NPs/MMC-SPC group and free MMC group ($P < 0.05$) (see Fig. S8†). Thus, the MTX-PEG-PE-PLA NPs/MMC-SPC showed a significantly enhanced therapeutic efficacy over the PEG-PE-PLA NPs/MMC-SPC and free MMC. Besides, the intravenous administration of the free MMC (4 mg/kg) resulted in the obvious listlessness/laziness and the pronounced body weight loss of mice (Fig. 8B), indicating the undesirable side effects of chemotherapy. All of the results suggested that the MTX-PEG-PE-PLA NPs/MMC-SPC were effective in improving therapeutic effectiveness of MMC remarkably with reducing its toxicity to synergize the therapeutic index.

The anticancer mechanisms of the MTX-PEG-PE-PLA NPs/MMC-SPC were further explained by histological examination. As shown in Fig. 8C, the tumors treated with 0.9% NaCl showed the extensive regions of tumor cells and intact vessels, implying the rapid tumor growth. In contrast, the nuclear shrinkage/fragmentation and injured vessels were presented in the free MMC, PEG-PE-PLA NPs/MMC-SPC or MTX-PEG-PE-PLA NPs/MMC-SPC-treated tumors, supporting the observation of the tumor growth inhibition.

The improved anticancer effect of the MTX-PEG-PE-PLA NPs/MMC-SPC while reducing their side effects was possibly due to the increasing intracellular internalization and accumulation of the targeted and pH-sensitive nanoscaled drug delivery systems at the target site. In this study, once the successful extravasation from the bloodstream into the tumor tissues (NPs size effect and PEG passive targeting), the nanoscaled drug delivery systems could efficiently enter the target cells through FA receptor-mediated endocytosis (MTX active targeting), escape the endo/lysosome, release the drug in a sustained/controlled state. The enhanced tumor accumulation and facilitated cellular uptake result in a rapid internalization and high accumulation of drug in the tumor cells. [50,51]

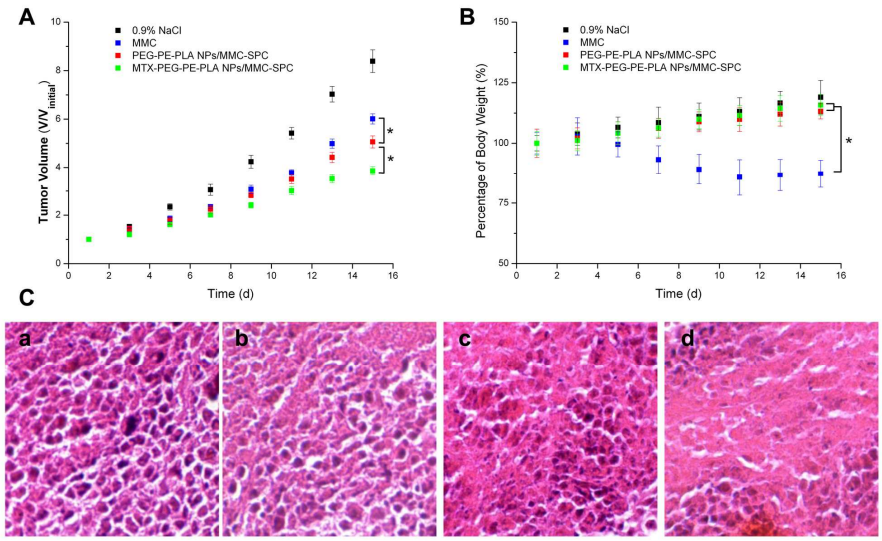

Fig. 8 In vivo anticancer effect of 0.9% NaCl, free MMC, PEG-PE-PLA NPs/MMC-SPC or MTX-PEG-PE-PLA NPs/MMC-SPC injected into H_{22} tumor-bearing mice at 4 mg/kg (MMC-eq. dose). (A) Tumor volume changes of H_{22} tumor-bearing mice treated with different groups (mean ± SD, n = 10). Statistical significance: * $P < 0.05$. (B) Body weight changes of H_{22} tumor-bearing mice treated

with different groups (mean ± SD, n = 10). (C) H&E staining of the tumor sections of H_{22} tumor-bearing mice treated with (a) 0.9% NaCl, (b) free MMC, (c) PEG-PE-PLA/MMC-SPC and (d) MTX-PEG-PE-PLA/MMC-SPC.

Conclusion

A new type of MTX-targeted and MMC-loaded PEG-PE-PLA hybrid NPs was developed using a lipid-MMC physical complex cooperated with a PEGylated lipid-MTX chemical conjugation for high encapsulation efficiency, sustained release characteristics, acceptable pharmacokinetics and improved therapeutic effect. This was the first work introducing the use of MMC-phopholipid complex to prepare the MMC-loaded polymer-lipid NPs. This work also systematically revealed the targeting effect of the MTX prodrug in vitro and in vivo. The targeting effect of these NPs resulted in the significantly elevated cellular uptake and enhanced cytotoxic activity against HeLa cells overexpressing the FA receptor. Moreover, the intravenous administration of these NPs in H_{22} tumor-bearing mice not only achieves the highly selective accumulation at the tumor site but also more efficiently inhibits the tumor growth in vivo.

Abbreviations used

MMC, mitomycin C; SPC, soybean phosphatidylcholine; MTX, methotrexate; ^{1}H NMR, proton nuclear magnetic resonance; UV-Vis, ultraviolet-visible spectroscopy; DLS, dynamic light scattering; ELS, electrophoretic light scattering; SEM, scanning electron microscopy; TEM, transmission electron microscopy; LCSM, laser confocal scanning microscopy; HPLC,

high-performance liquid chromatography; PDI, polydispersity index.

Acknowledgements

This work was supported by the National Natural Science Foundation of China (51373142) and the Scientific and Technical Project of Fujian Province of China (2009J1009).

Notes and references

1. V. N. Iyer and W. Szybalski, *Science*, 1964, **145**, 55-58.
2. M. Tomasz, R. Lipman, D. Chowdary, J. Pawlak, G. L. Verdine and K. Nakanishi, *Science*, 1987, **235**, 1204-1208.
3. W. T. Bradner, *Cancer Treat. Rev.*, 2001, **27**, 35-50.
4. S. Ekins, R. B. Kim, B. F. Leake, A. H. Dantzig, E. G. Schuetz, L.-B. Lan, K. Yasuda, R. L. Shepard, M. A. Winter, J. D. Schuetz, J. H. Wikel and S. A. Wrighton, *Mol. Pharmacol.*, 2002, **61**, 964-973.
5. S. Ekins, R. B. Kim, B. F. Leake, A. H. Dantzig, E. G. Schuetz, L.-B. Lan, K. Yasuda, R. L. Shepard, M. a. Winter, J. D. Schuetz, J. H. Wikel and S. A. Wrighton, *Mol. Pharmacol.*, 2002, **61**, 974-981.
6. P. Gontero, J. M. Sargent, D. J. Hopster, G. M. Lewandowic, C. G. Taylor, A. W. Elgie, C. J. Williamson, S. I. Sriprasad and G. H. Muir, *Anticancer Res.*, 2002, **22**, 4073-4080.
7. A. A. Gabizon, D. Tzemach, A. T. Horowitz, H. Shmeeda, J. Yeh and S. Zalipsky, *Clin. Cancer Res.*, 2006, **12**, 1913-1920.
8. K. W. Rumpf, J. Rieger, P. G. Lankisch, H. W. von Heyden, G. A. Nagel and F. Scheler, *Lancet*, 1980, **2**, 1037-1038.
9. J. den Hartigh, J. G. McVie, W. J. van Oort and H. M. Pinedo, *Cancer Res.*, 1983, **43**, 5017-5021.
10. J. A. Hubbell and A. Chilkoti, *Science*, 2012, **337**, 303-305.
11. D. Peer, J. M. Karp, S. Hong, O. C. Farokhzad, R. Margalit and R. Langer, *Nat. Nanotechnol.*, 2007, **2**, 751-760.
12. A. Gabizon, Y. Amitay, D. Tzemach, J. Gorin, H. Shmeeda and S. Zalipsky, *J. Controlled Release*, 2012, **160**, 245-253.
13. Z. Hou, Y. Li, Y. Huang, C. Zhou, J. Lin, Y. Wang, F. Cui, S. Zhou, M. Jia, S. Ye and Q. Zhang, *Mol. Pharmaceutics*, 2013, **10**, 90-101.
14. Z. Hou, H. Wei, Q. Wang, Q. Sun, C. Zhou, C. Zhan, X. Tang and Q. Zhang, *Nanoscale Res. Lett.*, 2009, **4**, 732-737.
15. J. Khan, A. Alexander, Ajazuddin, S. Saraf and S. Saraf, *J. Controlled Release*, 2013, **168**, 50-60.
16. J. H. Lee, K. J. Chen, S. H. Noh, M. A. Garcia, H. Wang, W. Y. Lin, H. Jeong, B. J. Kong, D. B. Stout, J. Cheon and H. R. Tseng, *Angew. Chem. Int. Ed.*,

2013, **52**, 4384-4388.
17. P. M. Kidd, *Altern. Med. Rev.*, 2009, **14**, 226-246.
18. M. A. Alam, F. I. Al-Jenoobi and A. M. Al-Mohizea, *Drug Discovery Today*, 2013, **18**, 936-949.
19. J. Shi, Z. Xiao, A. R. Votruba, C. Vilos and O. C. Farokhzad, *Angew. Chem. Int. Ed.*, 2011, **50**, 7027-7031.
20. S. Aryal, C.-M. Jack Hu, V. Fu and L. Zhang, *J. Mater. Chem.*, 2012, **22**, 994-999.
21. C. E. Ashley, E. C. Carnes, G. K. Phillips, D. Padilla, P. N. Durfee, P. A. Brown, T. N. Hanna, J. Liu, B. Phillips, M. B. Carter, N. J. Carroll, X. Jiang, D. R. Dunphy, C. L. Willman, D. N. Petsev, D. G. Evans, A. N. Parikh, B. Chackerian, W. Wharton, D. S. Peabody and C. J. Brinker, *Nat. Mater.*, 2011, **10**, 389-397.
22. C. Yuan, K. Raghupathi, B. C. Popere, J. Ventura, L. Dai and S. Thayumanavan, *Chem. Sci.*, 2014, **5**, 229-234.
23. P. S. Low, W. A. Henne and D. D. Doorneweerd, *Acc. Chem. Res.*, 2008, **41**, 120-129.
24. S. Rijnboutt, G. Jansen, G. Posthuma, J. B. Hynes, J. H. Schornagel and G. J. Strous, *J. Cell Biol.*, 1996, **132**, 35-47.
25. K. Mizusawa, Y. Takaoka and I. Hamachi, *J. Am. Chem. Soc.*, 2012, **134**, 13386-13395.
26. Q. Zhang, J. Zhu, L. Song, J. Zhang, D. Kong, Y. Zhao and Z. Wang, *J. Mater. Chem. B.*, 2013, **1**, 6402-6410.
27. G. Ling, P. Zhang, W. Zhang, J. Sun, X. Meng, Y. Qin, Y. Deng and Z. He, *J. Controlled Release*, 2010, **148**, 241-248.
28. X. Guo, C. Shi, J. Wang, S. Di and S. Zhou, *Biomaterials*, 2013, **34**, 4544-4554.
29. H. Wang, Y. Zhao, Y. Wu, Y. L. Hu, K. Nan, G. Nie and H. Chen, *Biomaterials*, 2011, **32**, 8281-8290.
30. E. Jin, B. Zhang, X. Sun, Z. Zhou, X. Ma, Q. Sun, J. Tang, Y. Shen, E. Van Kirk, W. J. Murdoch and M. Radosz, *J. Am. Chem. Soc.*, 2013, **135**, 933-940.
31. K. L. Young, C. Xu, J. Xie and S. Sun, *J. Mater. Chem.*, 2009, **19**, 6400-6406.
32. W. Gao, C.-M. J. Hu, R. H. Fang and L. Zhang, *J. Mater. Chem. B*, 2013, **1**, 6569-6585.
33. D. P. O'Neal, L. R. Hirsch, N. J. Halas, J. D. Payne and J. L. West, *Cancer Lett.*, 2004, **209**, 171-176.
34. N. Graf, D. R. Bielenberg, N. Kolishetti, C. Muus, J. Banyard, O. C. Farokhzad and S. J. Lippard, *ACS Nano*, 2012, **6**, 4530-4539.
35. M. V. Yezhelyev, L. Qi, R. M. O'Regan, S. Nie and X. Gao, *J. Am. Chem. Soc.*, 2008, **130**, 9006-9012.
36. Y. Zhao, X. Sun, G. Zhang, B. G. Trewyn, Slowing, II and V. S. Lin, *ACS Nano*, 2011, **5**, 1366-1375.
37. T. Yu, X. Liu, A. L. Bolcato-Bellemin, Y. Wang, C. Liu, P. Erbacher, F. Qu, P. Rocchi, J. P. Behr and L. Peng, *Angew. Chem. Int. Ed.*, 2012, **51**, 8478-8484.

38. S. Sengupta, D. Eavarone, I. Capila, G. Zhao, N. Watson, T. Kiziltepe and R. Sasisekharan, *Nature*, 2005, **436**, 568-572.
39. T. Jaskolla, B. Fuchs, M. Karas and J. Schiller, *J. Am. Soc. Mass Spectrom.*, 2009, **20**, 867-874.
40. H. Wu, L. Zhu and V. P. Torchilin, *Biomaterials*, 2013, **34**, 1213-1222.
41. Q. Xu, Y. Liu, S. Su, W. Li, C. Chen and Y. Wu, *Biomaterials*, 2012, **33**, 1627-1639.
42. X. Ma, H. Wang, S. Jin, Y. Wu and X. J. Liang, *Int. J. Nanomedicine*, 2012, **7**, 1313-1328.
43. S. Han, Y. Liu, X. Nie, Q. Xu, F. Jiao, W. Li, Y. Zhao, Y. Wu and C. Chen, *Small*, 2012, **8**, 1596-1606.
44. E. Fattal, P. Couvreur and C. Dubernet, *Adv. Drug Delivery Rev.*, 2004, **56**, 931-946.
45. J. Connor, M. B. Yatvin and L. Huang, *Proc. Natl. Acad. Sci. U. S. A.*, 1984, **81**, 1715-1718.
46. K. Li, D. Ding, D. Huo, K. Y. Pu, N. P. T. Ngo, Y. Hu, Z. Li and B. Liu, *Adv. Funct. Mater.*, 2012, **22**, 3107-3115.
47. X. L. Hu, R. Wang, J. Yue, S. Liu, Z. G. Xie and X. B. Jing, *J. Mater. Chem.*, 2012, **22**, 13303-13310.
48. Y. Zhang, H. Zhang, W. Wu, F. Zhang, S. Liu, R. Wang, Y. Sun, T. Tong and X. Jing, *Int. J. Nanomedicine*, 2014, **9**, 2019-2030.
49. S. Acharya and S. K. Sahoo, *Adv Drug Delivery Rev.*, 2011, **63**, 170-183.
50. Z. Gao, L. Zhang and Y. Sun, *J. Controlled Release*, 2012, **162**, 45-55.
51. R. Savic, L. Luo, A. Eisenberg and D. Maysinger, *Science*, 2003, **300**, 615-618.

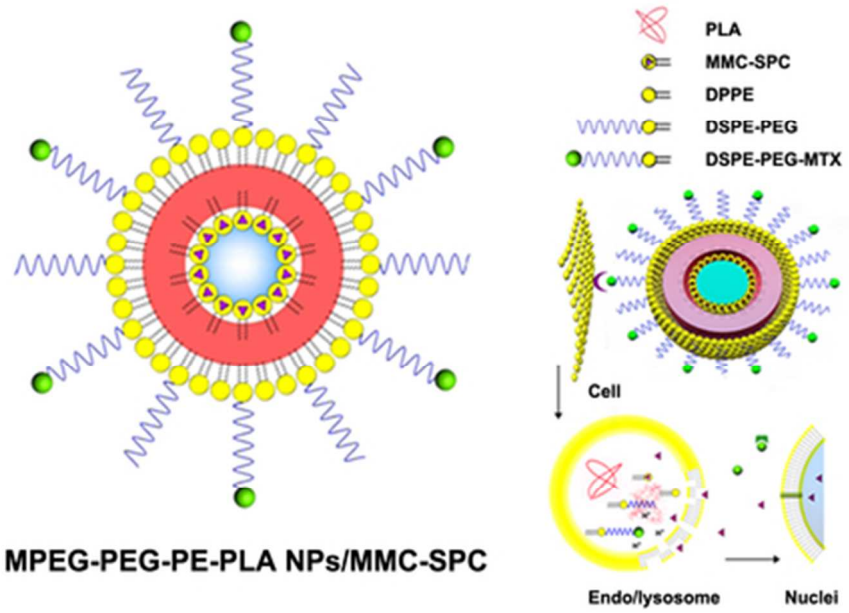

Lipid-MMC cooperated with PEGylated lipid-MTX based on PEG-PE-PLA hybrid NPs can coordinate an early-phase targeting effect with a late-phase anticancer effect
36x25mm (300 x 300 DPI)